

# Mixed-Mode Crack Propagation Calculations in a Pure Hexahedral Mesh

G. Dhondt<sup>1</sup>

**Abstract:** An algorithm is described which allows for the automatic calculation of crack propagation due to cyclic loading under mixed-mode conditions. The core of the procedure deals with the insertion of an arbitrarily formed crack into a virgin 20-node brick element mesh, thereby generating new quadratic bricks. One especially difficult aspect is the extension of the triangulation of the crack surface up to the boundary of the crack front elements. In the present article the technique is applied to linear elastic calculations using the stress intensity factor concept and a Paris-type law. However, other crack propagation parameters and crack propagation laws can be used equally well.

**keyword:** Crack,propagation,low cycle fatigue,mixed-mode,hexahedra

## 1 Introduction

Structures often fail by breaking into several parts. This implies that an initial crack has propagated either abruptly or due to cyclic loading. Here, the focus is on cyclic crack propagation. In industrial applications it is extremely important to be able to predict crack propagation. Indeed, material defects acting as initial cracks cannot always be avoided. These initial cracks will grow as two-dimensional surfaces in a three-dimensional body. Their shape depends on the loading characteristics, the geometry of the structure and the material properties. Generally, an initially plane crack can warp due to mixed-mode conditions. Therefore, a procedure to calculate crack propagation must be capable of dealing with arbitrarily curved crack shapes in three-dimensional space.

A lot of effort is still being spent to design such software. This treatise is not meant to be exhaustive. I would just like to attract the attention to a couple of different approaches. One of the first techniques used the bound-

ary element method [Wawrzynek, Martha, and Ingraffea (1988), Aliabadi (1997), Wen, Aliabadi, and Young (2004)]. This method looks very attractive since only the boundary of the structure has to be meshed. Indeed, one of the most difficult tasks in crack propagation calculations is the development of an automatic remeshing procedure, capable of coping with any feasible crack geometry. This problem is greatly reduced if meshing is limited to the free surface.

Alternatively, one can use extended finite elements [Gravouil, Moës, and Belytschko (2002)]. This is a recent technique, in which the crack propagation is independent of the mesh. Therefore, the method has similar advantages as the boundary element method, and this to an even higher degree: the problem of remeshing does not arise.

In another, more traditional approach the finite element method is used [Schöllmann, Fulland, and Richard (2003), Richard, Fulland, Buchholz, and Schöllmann (2002), Buchholz, Chergui, and Richard (2004)]. There, the crack front is surrounded by a flexible cylinder consisting of hexahedral elements, whereas the remaining space is filled with tetrahedral elements. In fact, the structure without crack is meshed with tetrahedra and only the immediate neighborhood of the crack front is remeshed.

Finally, there is the hexahedral technique developed at MTU and discussed in the present article. The technique has a long history: the first articles describing the procedure appeared in 1998 [Dhondt (1998)]. It has been applied to aero engine components on a regular basis since 1995. The technique has been proven to yield excellent results for Mode-I applications, exhibiting amazing capabilities describing crack propagation across corners and other geometric discontinuities [Dhondt (2005)]. An extension to real three-dimensional mixed-mode crack propagation calculations has long been proposed and applied to a three-point bending specimen. However, the artificial extension of the triangulation of the crack shape

---

<sup>1</sup> MTU Aero Engines, Postfach 50 06 40, D-80976 Munich, Germany

always remained a problem. In the present article, a new technique is presented to solve that problem and an overview is given of all necessary steps to apply the procedure. A couple of applications to the corner crack specimen illustrate the technique.

**2 Modification of the mesh**

To start, a suitable crack description must be chosen. Due to its flexibility and ease of operation it was decided to use a triangulation of the crack. Thus, the initial crack is triangulated at the start of the procedure, and each crack increment is triangulated as well and connected to the triangular mesh of the previous increment. Now, the problem is obviously reduced of inserting a triangular mesh into a 20-node brick mesh.

To this end, all edges of the 20-node brick mesh are catalogued according to whether they are cut by the triangulation or not. An edge of a 20-node brick element contains two end nodes and one middle node. If the intersection point on such an edge with the crack lies very close to one of the end nodes, all elements having this edge in common will be likely to yield very long and narrow or maybe very small elements after cutting. Thus, a first step aims at an improvement of the cutting geometry by moving the nodes of the intersected edges in such a way that the intersection point lies closer to the geometric middle point along the edge. Figure 1 shows how this mesh modification procedure works. Element edge  $p_3-p_4-p_5$  is cut by the triangulation in a point  $p_i$  close to  $p_3$ . The distances from the intersection point  $p_i$  to  $p_3$  and  $p_5$  are  $d_1$  and  $d_2$ , respectively. The nodes are labeled such that  $d_1 \leq d_2$ . The quantity  $d = (d_1 + d_2)/2$  is the mean of  $d_1$  and  $d_2$ . If  $|d - d_1|/d < 0.2$ , the intersection point is deemed close enough to the middle node and no modification is made. Else, the radii  $R_1 = (d_1 + d)/2$  and  $R_2 = (d_2 + d)/2$  are calculated for future use.

Whether  $p_3$  and  $p_5$  are really moved depends on the existence of suitable element edges  $p_1 - p_2 - p_3$  and  $p_5 - p_6 - p_7$ . Focusing on  $p_1 - p_2 - p_3$ , an element edge is looked for which:

1. does not belong to the elements containing edge  $p_3 - p_4 - p_5$ .
2. makes an angle  $\alpha \leq 60^\circ$  with the extension of  $p_3 - p_4 - p_5$  (Fig. 1).
3. is not cut twice or more by the triangulation.

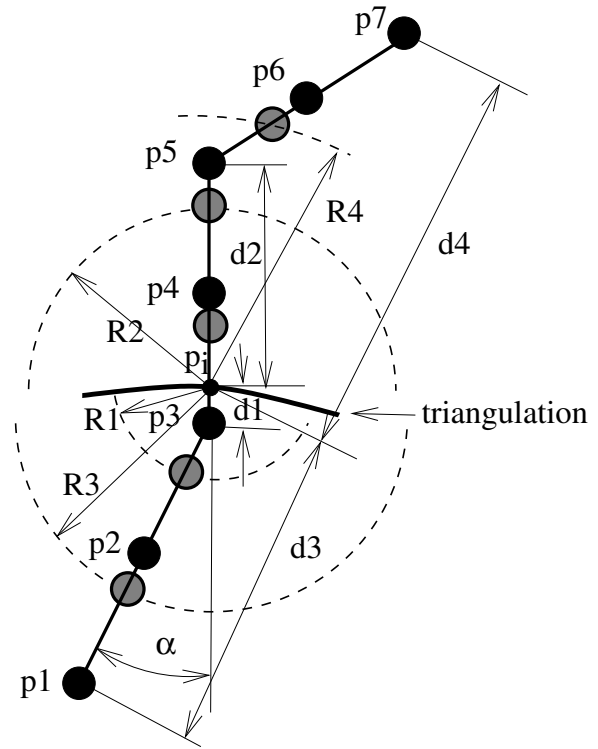


**Figure 1 : Mesh modification**

If no suitable edge  $p_1 - p_2 - p_3$  is found, node  $p_3$  is not moved. If more than one suitable edge is found, the one with the smallest  $\alpha$  is taken. If the search for  $p_1$  and  $p_2$  was successful, the distance  $d_3$  from  $p_1$  to the intersection point  $p_i$  is determined. If  $R_1 > 0.75d_3$ , which can occur if element edge  $p_1 - p_2 - p_3$  is much smaller than  $p_3 - p_4 - p_5$ , node  $p_3$  is not moved. Finally,  $R_3$  is determined by  $R_3 = (d_3 + R_1)/2$  and node  $p_3$  is moved to a position on  $p_1 - p_2 - p_3$  on a distance  $R_1$  from  $p_i$ , node  $p_2$  is moved onto a distance  $R_3$  from  $p_i$ . Ultimately, the same procedure applies to element edge  $p_5 - p_6 - p_7$ . Finally, all midside nodes not already moved belonging to any edges of which one of the end nodes was moved, are moved into the middle of their end nodes. The new position of  $p_2, p_3, p_4, p_5$  and  $p_6$  is shown by the grey circles in Fig. 1.

**3 Extension of the triangulation**

Not all elements of the uncracked mesh are completely cut. Those elements which contain the crack front are only partially cut. For the subsequent procedure it is important that each element is either completely cut, or not

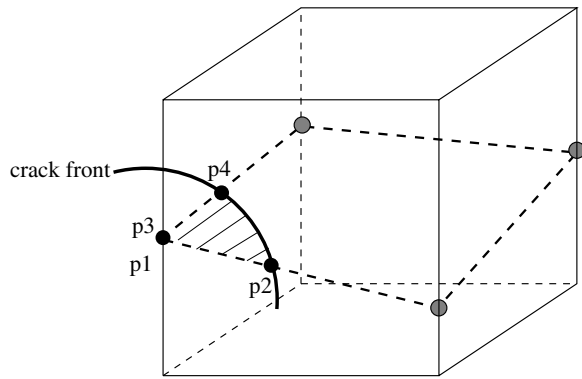


Figure 2 : Crack front element (topology 1)

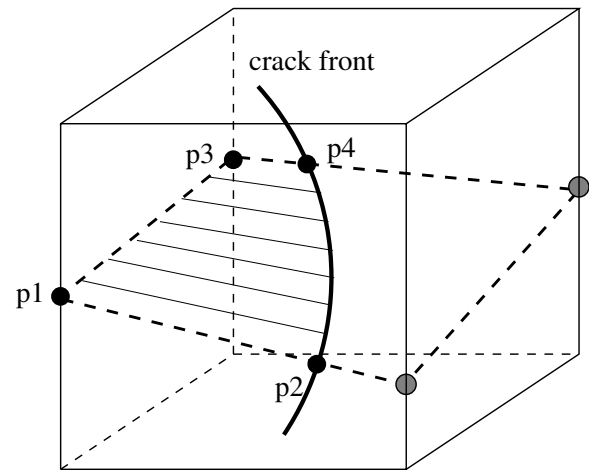


Figure 3 : Crack front element (topology 2)

cut at all. Therefore, for elements containing the crack front the cutting produced by the triangulation has to be extended into the complete element.

The procedure to do so is explained in Fig. 2. It shows a crack front element, i.e. an element cut by the crack front. The front cuts two faces of the element in points  $p_2$  and  $p_4$ . Let us call these faces crack front faces and the points crack front points. The crack front points are found by calculating the intersection of a coarse triangulation of the element faces with a piecewise straight approximation of the crack front. In the figure the triangulation is represented by the shaded area. It is assumed that a crack front element contains at most two crack front points. Fig. 3 and Fig. 4 show two other possibilities in which a crack front element can be cut by the crack front. If a crack front element is cut more than twice by the crack front a finer mesh should be used for the uncracked structure.

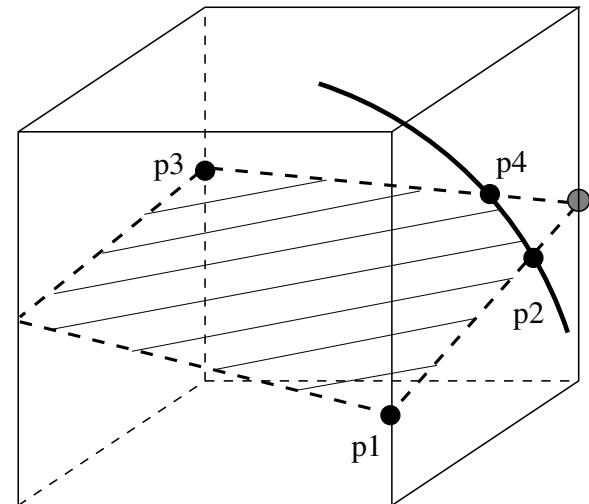


Figure 4 : Crack front element (topology 3)

Within each crack front face the triangulated crack shape cuts exactly one of the face's vertices. The intersection point for the face containing  $p_2$  is called  $p_1$ , the intersection point for the face containing  $p_4$  is called  $p_3$ . Now, the crack shape is extended within the crack front element by defining a bilinear function through the points  $p_1 - p_2 - p_4 - p_3$ . This is shown by the thick dashed lines in Fig. 2-Fig. 4 and illustrated schematically in Fig. 5. Notice that the defining points can be degenerated to a set of only three distinct points (Fig. 2). The extension is described by the local coordinates  $u$  and  $v$  running from  $p_4$  to  $p_3$  and from  $p_4$  to  $p_2$ , respectively. The extension cuts some additional edges of the crack front elements symbolized by the gray circles in Fig. 2-Fig. 4. Notice that although the edges in the figures are straight, this does not

necessarily have to be the case. The intersection of the bilinear shape with a quadratic edge of a 20-node brick element, represented by  $q_1 - q_2 - q_3$  in Fig. 5 is found by solving the following nonlinear set of equations:

$$(1-u)(1-v)\mathbf{p}_4 + u(1-v)\mathbf{p}_3 + uv\mathbf{p}_1 + v(1-u)\mathbf{p}_2 = \frac{1}{2}(\mathbf{q}_1 - 2\mathbf{q}_2 + \mathbf{q}_3)w^2 + \frac{1}{2}(\mathbf{q}_3 - \mathbf{q}_1)w + \mathbf{q}_2, \quad (1)$$

where the boldface symbols stand for the vectors corresponding to the points and  $w$  is a parameter between -1 and +1. This set of equations can be solved using a standard Newton-Raphson procedure.

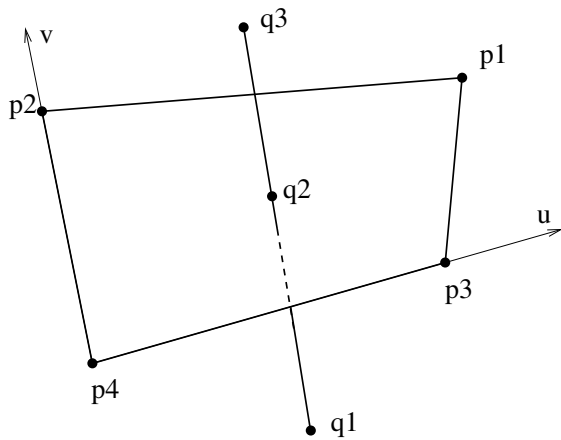


Figure 5 : Determination of new cutting points

Summarizing, the extension of the crack shape throughout the complete crack front elements involves the following steps:

1. determining the intersection of the mesh with the crack front, leading to the crack front elements, crack front faces and crack front points  $p_2$  and  $p_4$ .
2. calculating the intersection of the edges of the crack front faces with the triangulated crack shape: this yields points  $p_1$  and  $p_3$ . Points  $p_1$  to  $p_4$  define a bilinear shape which is used as an extension of the crack shape.
3. cutting the extended shape with all edges of the crack front element.

Two different, adjacent crack front elements share one crack front face. If there is only one crack front, then  $n$  crack front elements correspond to  $n + 1$  crack front faces. Problems can arise if two different crack front faces share the same edge. This is illustrated in Fig. 6.

The bilinear extension of the crack surface in element 1 is determined by points  $p_1 - p_2 - p_3 - p_4$ . It cuts edge  $p_a - p_b$ , which belongs to one of the crack front faces of element 1, in point  $i_1$ . The bilinear extension of the crack surface in element 2, which is adjacent to element 1, is defined by points  $p'_1 - p'_2 - p'_3 - p'_4$ . It cuts edge  $p_a - p_b$ , which belongs to both crack front faces of element 2, in point  $i_2$ . Since the crack front faces are not necessarily plane, the points  $i_1$  and  $i_2$  can be different: the extension

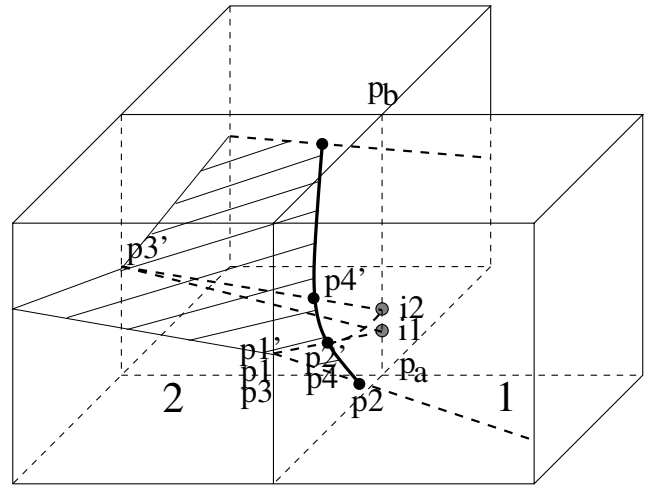


Figure 6 : Two different crack front faces sharing an edge

of the crack surface, as outlined before, is not necessarily continuous across element boundaries.

To resolve this problem the crack front elements are ordered according to their adjacency. The crack front faces are determined and edges belonging to different crack front faces are singled out. Then, the crack front elements are treated in their adjacency order. Focussing on Fig. 6, the crack front points  $p_2$  and  $p_4$  for element 1 are determined, followed by the crack shape intersection points  $p_1$  and  $p_3$ . Subsequently, a check is performed whether any crack front face of the element at stake contains a common edge. This is the case for the crack front face to which  $p_4$  belongs, since it contains edge  $p_a - p_b$ . Now, the point on the straight line through  $p_a$  and  $p_b$  closest to the straight line through  $p_1$  and  $p_4$  is determined (in Fig. 6 this is point  $i_1$ ) and used in the bilinear extension instead of point  $p_4$ . This means that the bilinear extension in element 1 is now based on  $p_1 - p_2 - p_3 - i_1$  instead of  $p_1 - p_2 - p_3 - p_4$ . For element 2 a similar procedure is applied: first, the crack front points  $p'_2, p'_4, p'_1$  and  $p'_3$  are determined. Then, a check is made whether the crack front faces which belong to the element contain any common edges. This is the case for both crack front faces: both of them contain edge  $p_a - p_b$ . A check of the data base reveals that this common edge has already been cut in point  $i_1$ . This point replaces points  $p'_2$  and  $p'_4$  in the bilinear extension in element 2. Consequently, the bilinear extension in element 2 is based on  $p'_1 - i_1 - p'_3 - i_1$ . This guarantees a continuous extension across neighbor-

ing elements.

Summarizing, the procedure now reads:

1. determine the intersection of the crack front with all elements, leading to the crack front elements, crack front faces and crack front points  $p_2$  and  $p_4$ .
2. sort the crack front elements according to their adjacency.
3. check for common edges, i.e. edges belonging to two different crack front faces and catalogue them.
4. start a loop over all crack front elements in adjacency order performing the following actions:
  - (a) determine the intersection of the edges belonging to the crack front faces with the crack shape triangulation leading to points  $p_1$  and  $p_3$ .
  - (b) check whether any crack front face belonging to the element contains a common edge. If this is not the case, do nothing. Else, if the common edge has not yet been encountered during the treatment of a previous crack front element, the point on the common edge closest to the line through points  $p_1$  and  $p_2$  or  $p_3$  and  $p_4$  (depending on the crack front face) is determined and called the common edge intersection point. Subsequently, the crack front point is replaced by the common edge intersection point in the bilinear crack extension definition.
  - (c) determine the intersection of the bilinear crack extension with those edges which have not been intersected yet.

#### 4 Cutting topologies

After the crack triangulation has been extended to the boundaries of the crack front elements, all cut elements are catalogued according to the way in which they are cut. A distinction is made between simple and complex cutting topologies. A topology is simple if the following two conditions are satisfied:

1. each edge of the element is cut at most once by the triangulation
2. the topology leads to at most two parts after cutting.

In general, both conditions are satisfied in fracture calculations since the fracture surface is usually smooth and does not exhibit high curvature. If this is not the case a finer mesh for the uncracked structure should be used. To determine the category to which a specific element belongs, all vertex nodes of the element are labeled with 0 or 1, according to whether the node lies on the one side of the crack shape or on the other side. If there are more 1's than 0's the labels are reversed. The vertex nodes in Fig. 7 with the black circles represent 1, the other 0. Thus, comparison with the schematic drawings in Fig. 7 allows for a unique classification of the element at stake. The notation 1-7 in Fig. 7 means that one corner node lies on one side of the triangulation, whereas all other seven nodes lie on the other side. The numbers in brackets show the number of variations for each scheme. For instance, for topology 1-7(a) there are eight ways in which to choose a corner node.

There is only one simple topology for cases 1-7, 2-6 and 3-5. Case 4-4 corresponds to four simple topologies. For each of the simple topologies a remeshing scheme has been developed satisfying the following requirements:

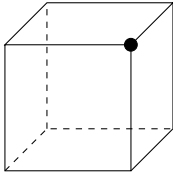
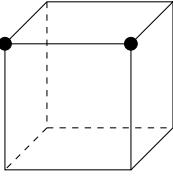
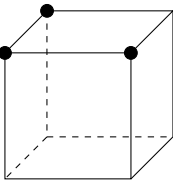
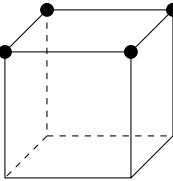
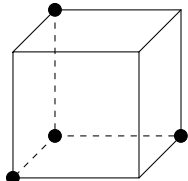
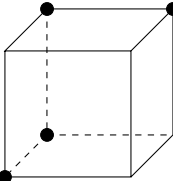
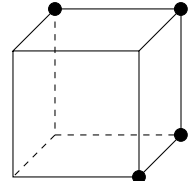
1. only genuine 20-node brick elements are generated,
2. compatibility between different topologies is assured.

The ensuing remeshing schemes are similar to the mid-point subdivision proposed by Li et al [Li, McKeag, and Armstrong (1995)]. However, the new nodes in the middle of the faces are generated using slightly different rules to improve the shape of the resulting elements. The remeshing for topology 1-7 is shown in Fig. 8 and Fig. 9. For the other schemes the reader is referred to [Dhondt (2001)].

In all schemes only genuine 20-node brick elements are generated without recourse to tetrahedra or other element types. All faces of the newly generated elements have four different corner nodes. Furthermore, by remeshing topologically identical faces of the mother element in exactly the same way, compatibility between different topologies is guaranteed.

#### 5 Inserting the crack front

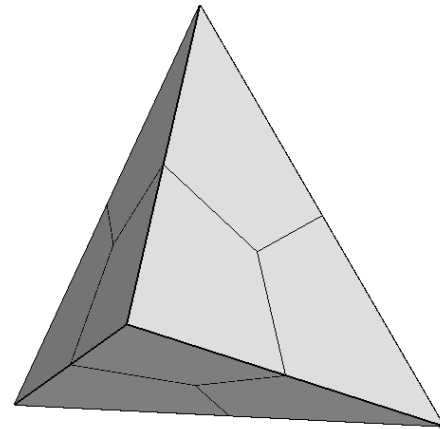
At this stage the crack shape has been inserted into the mesh. Now, the crack front can be modeled. To this

1-7 (8)	 a (8)
2-6 (12)	 a (12)
3-5 (24)	 a(24)
4-4 (38)	<div style="display: flex; justify-content: space-around;"> <div style="text-align: center;">                       a (6)                 </div> <div style="text-align: center;">                       b (8)                 </div> </div>
	<div style="display: flex; justify-content: space-around;"> <div style="text-align: center;">                       c (12)                 </div> <div style="text-align: center;">                       d (12)                 </div> </div>

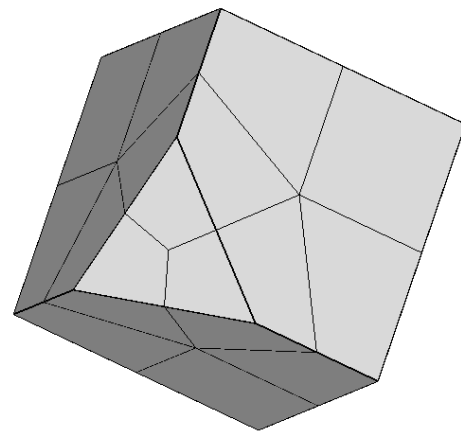
**Figure 7 :** Classification of the simple topologies

end, all elements adjacent to the crack front are identified. What follows is again a two-step procedure. First, the edges of the elements are moved to improve the cutting geometry. Then, the elements are remeshed.

The modification of the element edges is necessary to assure that the geometry of the elements after remeshing is not too bad. This is illustrated in Fig. 10 and Fig. 11. A plane crack shape is used to simplify the visualization. In



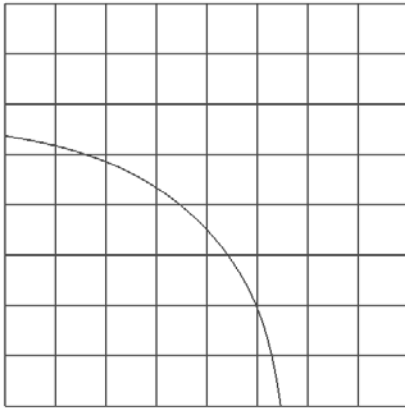
**Figure 8 :** Remeshing topology 1-7



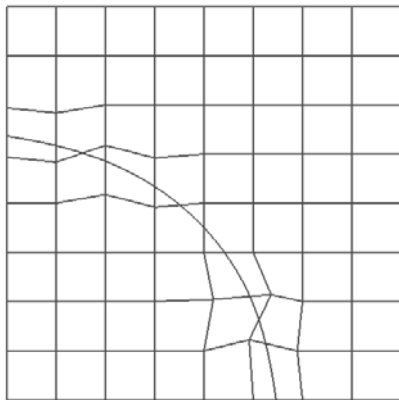
**Figure 9 :** Remeshing topology 1-7

Fig. 10 some of the elements are cut in a rather bad way: either very small or long and narrow elements will result after cutting. By moving the edges of the elements using a method similar to the one in section 2 the position of the elements with respect to the crack front is much improved, Fig. 11. Of course, care must be taken that the crack nodes stay in the crack shape during the modification.

After the modification of the element boundaries surrounding the crack front, crack-tip elements can be generated. This involves the creation of collapsed elements at the crack tip, surrounded by a few concentric layers of regular elements, thus ensuring the correct calculation of the asymptotic stress field. For the collapsed elements



**Figure 10** : Mesh before modification



**Figure 11** : Mesh after modification

the so-called quarter-point elements (with the crack-tip nodes kept together) are taken, yielding a  $1/\sqrt{r}$  strain singularity at the crack tip [Barsoum (1976)].

Looking at Fig. 12 and Fig. 13 it is noticed that the crack front can cut the element faces in two different ways: either two opposite edges are cut or two edges meeting in a common node. Other, more fancy cases can be thought of, for instance a crack front cutting one edge of a face twice. However, this seldom occurs in practice and can be avoided by choosing a finer mesh.

In case two opposite edges are cut, the element subdivision is performed according to Fig. 12. At the crack front three crack-tip elements are generated, surrounded by a couple of layers (the amount of layers can be determined by the user) of regular elements. Notice that new end nodes have been generated on three faces of the original

element only. In particular, the face of the element opposite to the one in the crack plane has not been changed. Consequently, the mesh refinement is restricted to one layer of elements on each side of the crack plane. All new nodes are obtained by linear interpolation, the only exception being the new middle nodes along the crack front which are in addition projected onto the crack front. If the projection leads to degenerate elements (marked by a negative Jacobian in at least one of the integration points) it is not performed.

The second case is shown in Fig. 13 and can be reduced to the first case by bisecting the element along a diagonal plane through the common node of the intersected edges. The resulting halves are upgraded to 20-node elements by expanding the edge through the common node and not part of the crack plane into a face by repeatedly using the nodes on this edge in the topology of the new elements. Each of the new elements is now meshed following the scheme of Fig. 12. At this point two important comments on the second case are due. First, the division of the element in two halves requires the generation of an additional mid-side node on the face opposite to the one in the crack plane. This node should be linked to the side nodes of this face using a multiple point constraint. Second, at the common node (Fig. 13) collapsed half-point elements are generated with nodes which are kept together at the collapsed face. It can be shown that this type of element does not exhibit a singular behaviour at the collapsed face [Dhondt (1993)].

With the above algorithm all elements which are cut by the crack front are remeshed to yield crack-tip elements. This information is collected into a new input deck for the finite element program. It is clear that all other information in the uncracked structure which was attached to the elements which are being remeshed has to be redistributed too. This applies, for instance, to pressure loading attached to the surface.

## 6 Crack propagation

Using the technique explained in the previous sections, the stress distribution at the crack tip can be determined by a generic finite element code, e.g. CalculiX [Dhondt and Wittig (1998-2005)]. By comparing this stress field with the analytical asymptotic stress field the stress intensity factors  $K_I$ ,  $K_{II}$  and  $K_{III}$  can be determined [Dhondt (2002)]. Based on these stress intensity factors the Sih criterion [Richard (1985)] yields a crack propagation di-

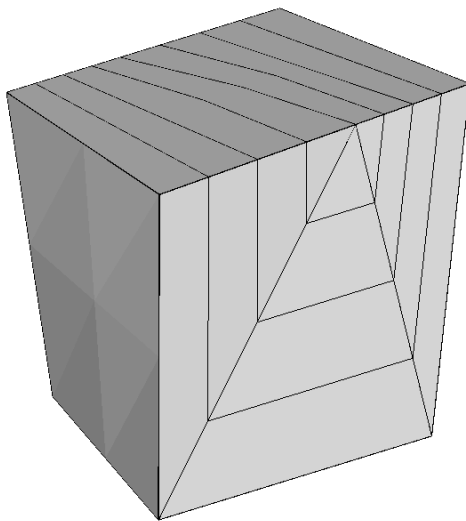


**Figure 12 :** Mesh refinement at the crack front for a crack cutting two opposite sides of an element

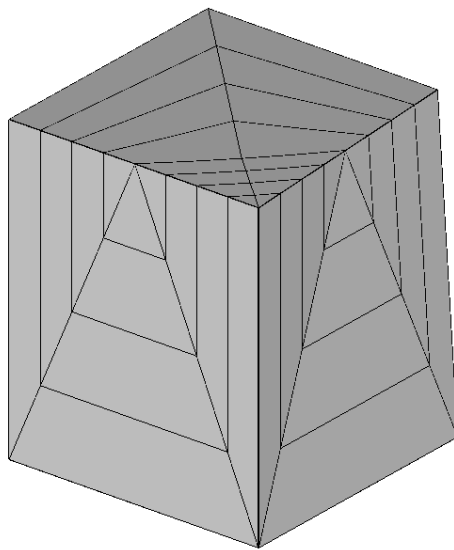


**Figure 13 :** Mesh refinement at the crack front for a crack cutting two sides having a node in common

rection and an equivalent stress intensity factor. Substituting this equivalent factor into the Paris law leads to a crack increment size. However, other criteria and other crack propagation laws exist and the most appropriate criterion and law may depend on the application.

Once a new crack front was determined, the whole procedure can start over again. However, in practice, the crack propagation increment due to one cycle is very small (e.g.

$10^{-4}$  mm/cycle) leading to a K-distribution which is only marginally different from the original one. Furthermore, the difference is probably smaller than the numerical inaccuracies involved. Therefore, it is more appropriate to calculate the crack propagation for  $N > 1$  cycles leaving the K-distribution constant during these  $N$  cycles. In the calculations performed with the present method it has proven fruitful, instead of keeping  $N$  fixed during the complete crack propagation calculation from initial crack to rupture, to fix the maximum allowed crack propagation increment along the crack front (in units of length). Since the crack propagation increases for increasing K-values, the location along the crack with the highest K-values will dictate the number of cycles.

Although the preceding paragraph indicates that the calculation of the new crack front is relatively simple, the crack propagation process is additive and can easily lead to instabilities. Each step uses the information of the previous one and one slightly jumpy K-distribution can be enough to jeopardize the iteration steps to follow. A lot of time and trial and error was spent to create a robust procedure. It consists of several steps. The procedure reads as follows:

## 7 Examples

1. First, the original crack shape and the finite element crack geometry are read. The original shape is assumed to be piecewise quadratic, except at the start of the calculation, where it can also be straight or elliptical. It generally does not stop at the free surface of the structure and penetrates to some extent into free space. The finite element geometry contains the nodes on the crack front and is a piecewise quadratic approximation to the original crack shape. It starts and ends exactly at the intersection of the original crack shape with the free surface.
2. The K-distribution at the crack front is calculated from the stresses in the reduced integration points ahead of the crack tip and plotted along the crack front. Sometimes this distribution exhibits some irregular behavior, e.g. a zig-zag or erroneous values due to a particularly bad geometry. Especially, the end points of the crack front are more prone to error than the subsurface points. To remove the zig-zag in a node, the K-value in this node is replaced by the mean of itself and the value it would get by lin-



early connecting its neighbors. The end nodes are replaced by linear extrapolation from the two most close subsurface neighbors. In addition, a B-spline approximation is performed.

3. In the next step,  $2n + 1$  equidistant sample points are taken along the finite element crack front and projected on the original crack shape to ensure the greatest possible accuracy. The K-values in those sample points are obtained by evaluation of the B-spline determined in the previous step. The number of sample points should be chosen such that a spline approximation through the sample points models the original shape with sufficient accuracy. The examples in the next section were calculated with  $n=49$ .
4. In the sample points the crack propagation direction is calculated. For subsurface points this is in a plane normal to the original crack shape, for surface points it is within the free surface. However, for geometrically widening components, where the tangent plane at the free surface in propagation direction may cut the structure this would lead to a new crack front not intersecting the free surface any more. Therefore, the tangent plane at the free surface is rotated about a straight line in its plane and locally perpendicular to the crack shape over  $\pi/8$  into free space and the crack propagation increment is appropriately increased in magnitude in order to ensure the correct crack propagation at the free surface.
5. Based on the maximum allowed crack propagation increment along the crack front, the number of cycles is determined and a new crack shape is calculated. This shape should intersect the free surface of the structure and penetrate to some extent into free space.
6. The new crack shape is represented in polar coordinates (with the origin located somewhere within the crack) and a B-spline smoothing is performed.
7. Finally, a set of  $2n + 1$  equidistant points is determined on the smoothed contour yielding a piecewise quadratic propagated crack shape suitable as input for the next calculation. The equidistance of the points increases the numerical stability of the next

iteration. Again, for the examples in the next section  $n=49$  was taken.

In this section, three examples are discussed. The geometry in all examples is the same: it is the middle section of a corner crack specimen and measures  $8 \times 8 \text{ mm}^2$  in cross section. The initial crack is straight and has a crack depth of 2.5 mm.

In the first example the loading is a pure tensile force, leading to mode I conditions at the crack tip. The tensile stress in the deformed configuration is shown in Fig. 14.

Fig. 15 shows some crack propagation fronts whereas in Fig. 16 the crack length is plotted versus the number of cycles. It is well known that the stress intensity factors for a straight crack in a corner crack specimen attain their maximum in the middle of the specimen, and drop towards the free surface. Therefore, the crack propagation is more pronounced in the middle of the specimen. During the calculation the maximum crack propagation increment was increased at a certain point to reduce the computational time. This corresponds to the jump in crack front density visible in Fig. 15. Notice that, apart from the jump, the maximum crack propagation increment is kept constant and not the number of cycles. In fact, for a constant crack propagation increment the number of cycles steadily decreases while the crack propagates. This can also be seen in Fig. 16.

In the second example an additional force parallel to the crack plane and perpendicular to the crack front was added. This leads to an additional symmetric  $K_{II}$  distribution and a small  $K_{III}$  contribution (Fig. 17).

Due to mode-II the crack turns. This is most clear at the free surface, where the  $K_{II}/K_I$  ratio is highest. Fig. 18 shows the mesh for the largest crack front (cut along the crack) and Fig. 19 shows the triangulation of the crack at that stage. During propagation each crack increment is triangulated separately and connected to the triangulation of the previous crack. The highest deviation from the crack plane takes place at the start of the calculation.

The third example involves opposite forces of the kind applied in example two. This basically leads to torsion. This is clearly visible in Fig. 20, which shows the mesh for the last crack front and Fig. 21, which depicts the triangulation.

At one free surface the crack turns upwards, at the other it turns downwards.

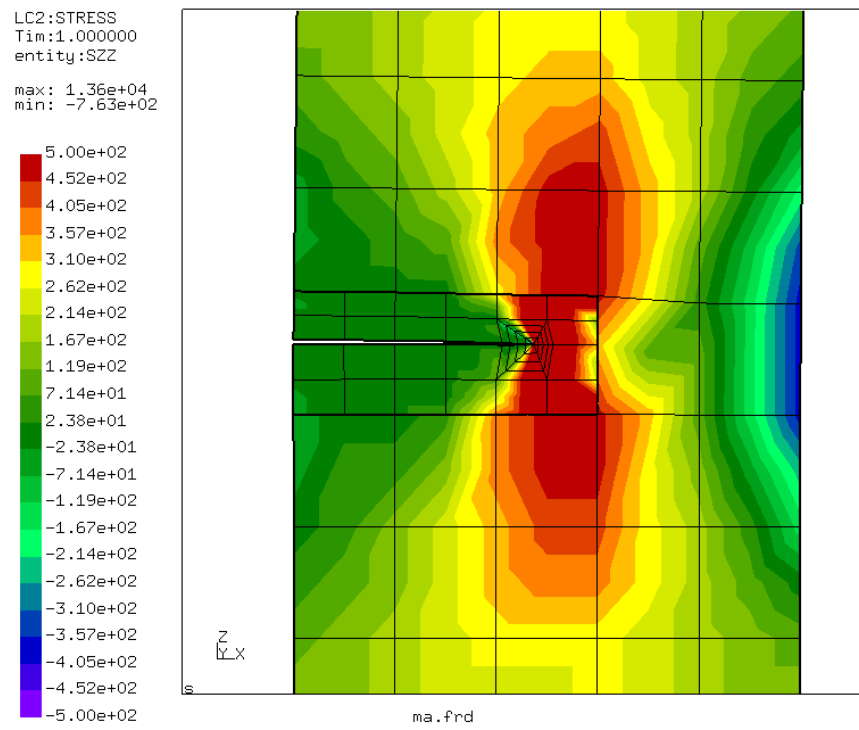


Figure 14 : Normal stress on the crack plane

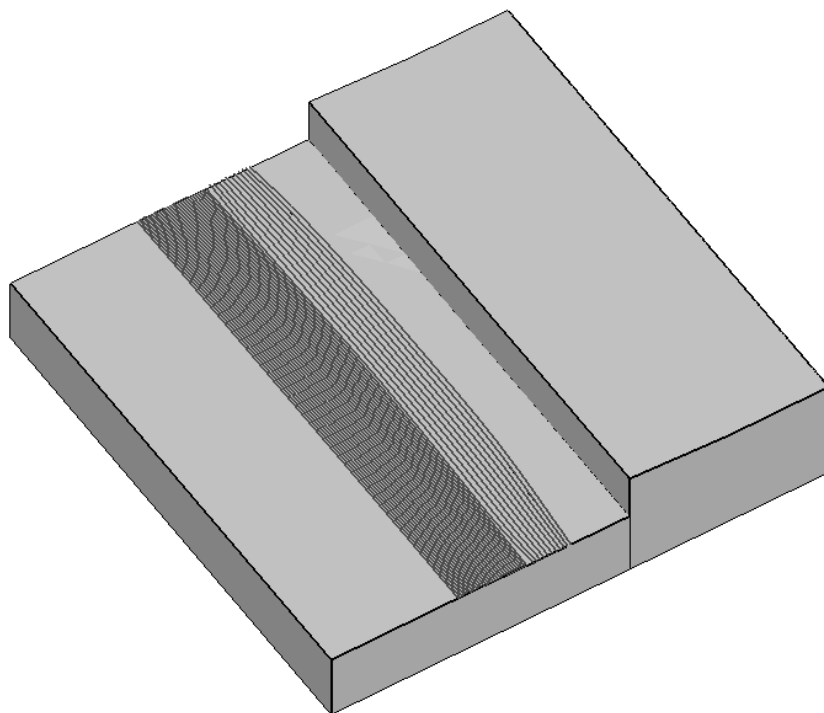


Figure 15 : Crack fronts during propagation

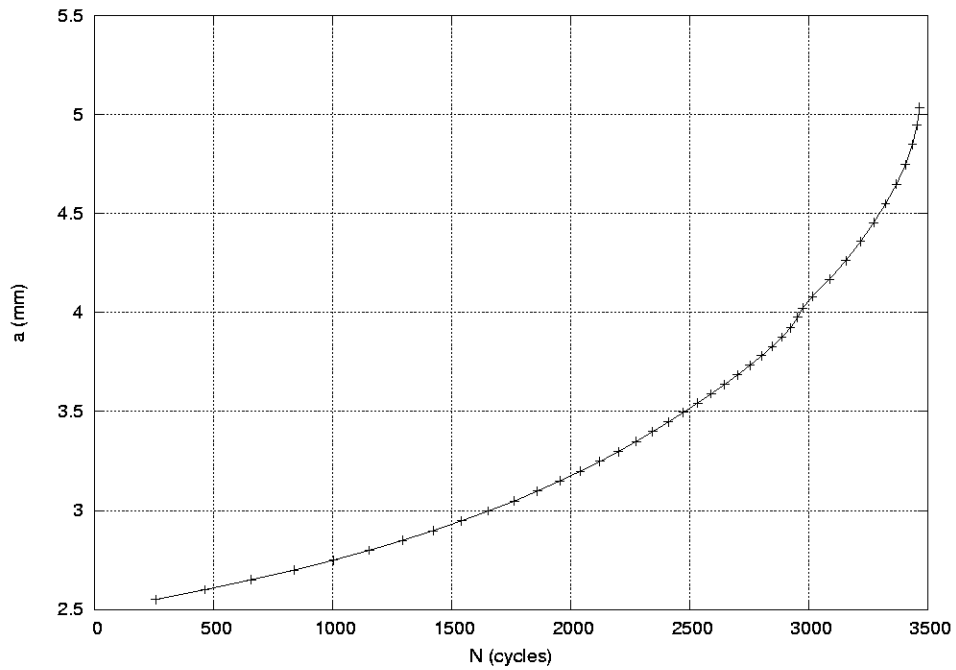


Figure 16 : Crack length versus number of cycles

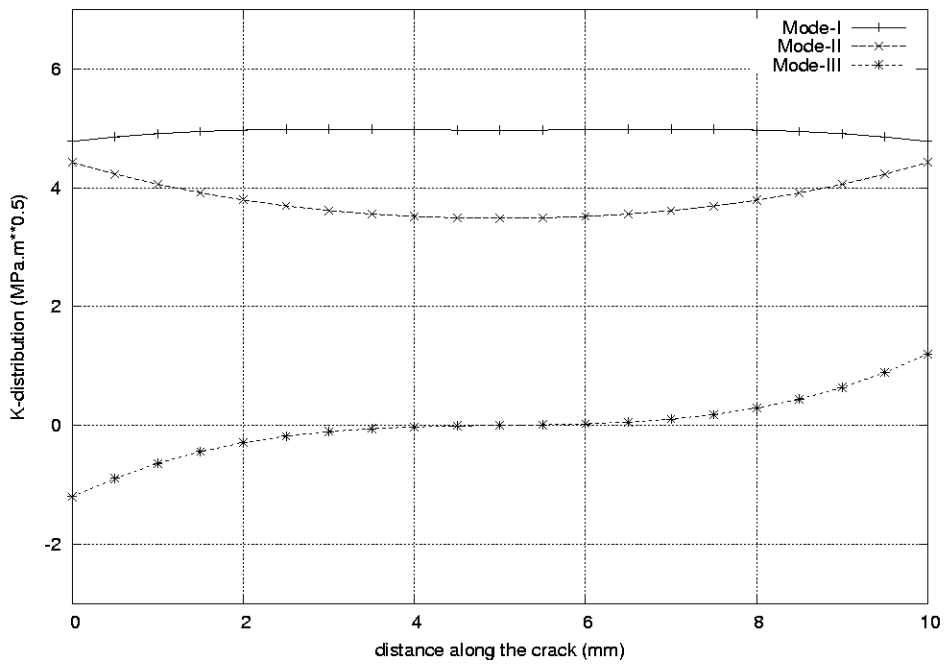
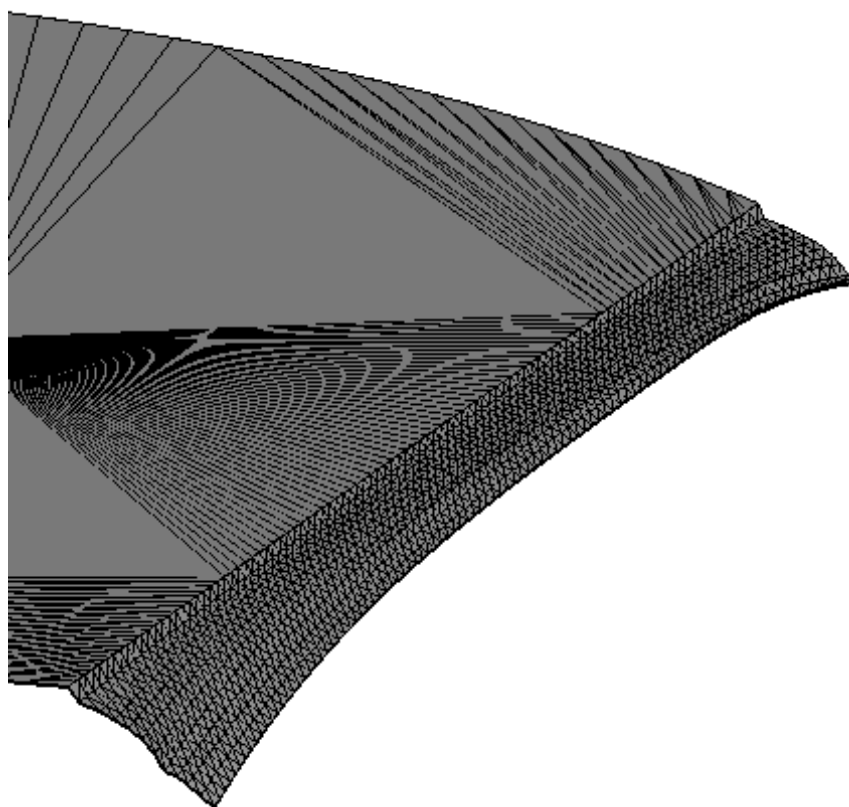
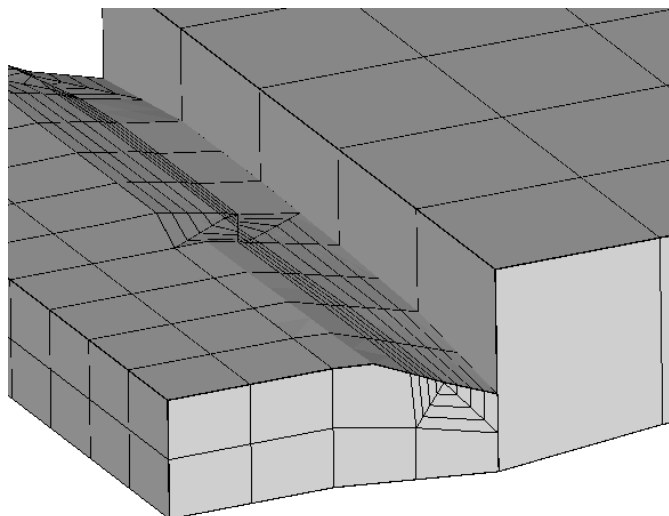
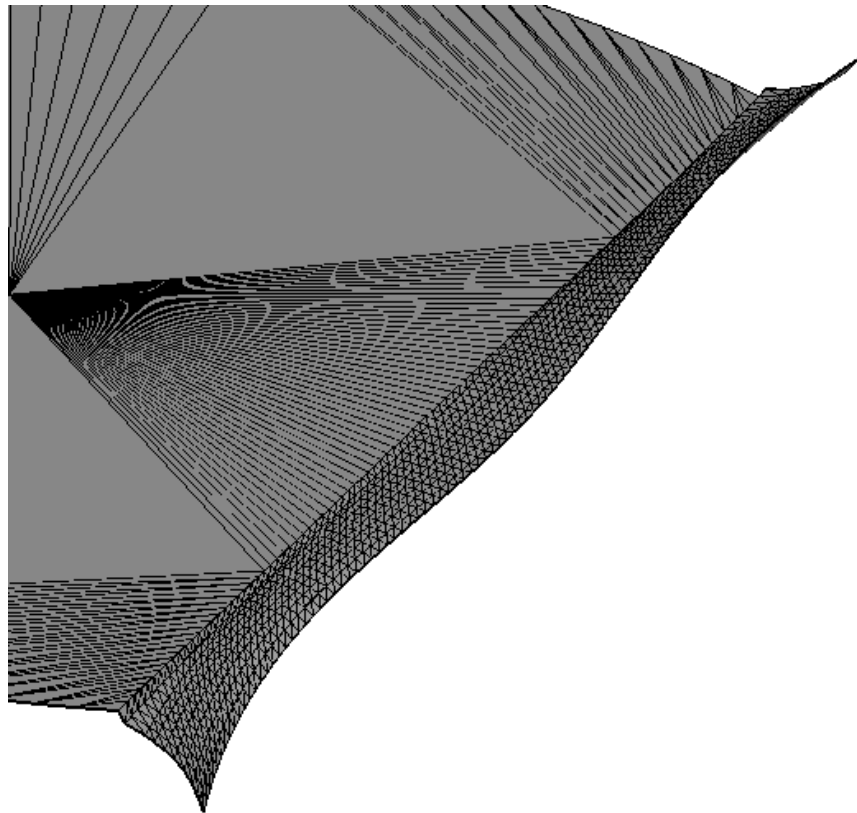


Figure 17 : K-distribution along the initial crack (example 2)

**Figure 18** : Mesh for the largest crack front (example 2)



**Figure 19** : Triangulation of the largest crack (example 2)



**Figure 21** : Triangulation of the largest crack (example 3)

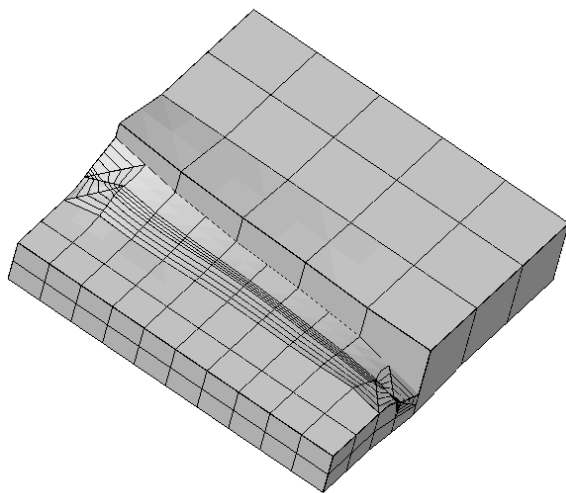


**Figure 20** : Mesh for the largest crack front (example 3)

## 8 Conclusions

The method developed at MTU to calculate mixed-mode crack propagation was enhanced by including an appro-

priate crack shape extension procedure. This removes the need to extend the crack shape through the whole structure. The applications show that the procedure works well for simple specimens. The next step is the application to real components.

## References

**Aliabadi, M. H.** (1997): A new generation of boundary element methods in fracture mechanics. *Int. J. Fract.*, vol. 86, pp. 91–125.

**Barsoum, R. S.** (1976): On the use of isoparametric finite elements in linear fracture mechanics. *Int. J. Num. Meth. Engng.*, vol. 10, pp. 25–37.

**Buchholz, F.-G.; Chergui, A.; Richard, H. A.** (2004): Fracture analyses and experimental results of crack growth under general mixed mode loading conditions. *Engineering Fracture Mechanics*, vol. 71, pp. 455–468.

- Dhondt, G.** (1993): General Behaviour of Collapsed 8-Node 2-D and 20-Node 3-D Isoparametric Elements. *Int. J. Num. Meth. Engng.*, vol. 36, pp. 1223–1243.
- Dhondt, G.** (1998): Automatic 3-D Mode I crack propagation calculations with finite elements. *Int. J. Num. Meth. Engng.*, vol. 41, pp. 739–757.
- Dhondt, G.** (2001): A new automatic hexahedral mesher based on cutting. *Int. J. Num. Meth. Engng.*, vol. 50, pp. 2109–2126.
- Dhondt, G.** (2002): Mixed-Mode K-Calculations in Anisotropic Materials. *Engng. Fract.Mech.*, vol. 69, pp. 909–922.
- Dhondt, G.** (2005): Cyclic crack propagation at corners and holes. *Fatigue Fract. Engng. Mater. Struct.*, vol. 28, pp. 25–30.
- Dhondt, G.; Wittig, K.** (1998-2005): *CalculiX: A Free Software Three-Dimensional Structural Finite Element Program.* www.calculix.de.
- Gravouil, A.; Moës, N.; Belytschko, T.** (2002): Non-planar 3D crack growth by the extended finite element method and level sets Part II: level set update. *Int. J. Num. Meth. Eng.*, vol. 53, pp. 2569–2586.
- Li, T. S.; McKeag, R. M.; Armstrong, C. G.** (1995): Hexahedral meshing using midpoint subdivision and integer programming. *Comput. Methods Appl. Mech. Engrg.*, vol. 124, pp. 171–193.
- Richard, H. A.** (1985): *Bruchverhersagen bei überlagerter Normal- und Schubbeanspruchung von Rissen, Bericht 631/85.* VDI Verlag.
- Richard, H. A.; Fulland, M.; Buchholz, F.-G.; Schöllmann, M.** (2002): 3D Fracture Criteria for Structures with Cracks. *Steel research*, vol. 74(8), pp. 491–497.
- Schöllmann, M.; Fulland, M.; Richard, H. A.** (2003): Development of a new software for adaptive crack growth simulations in 3D structures. *Engng. Fract. Mech.*, vol. 70, pp. 221–230.
- Wawrzynek, P. A.; Martha, L. F.; Ingraffea, A. R.** (1988): A Computational Environment for the Simulation of Fracture Processes in Three Dimensions. *Analytical, Numerical and Experimental Aspects of Three Dimensional Fracture Processes*, ed. A. J. Rosakis et al., ASME AMD, vol. 91, pp. 321–327.
- Wen, P. H.; Aliabadi, M. H.; Young, A.** (2004): Crack growth analysis for multi-layered airframe structures by boundary element method. *Engng. Fract. Mech.*, vol. 71, pp. 619–631.